ACS APPLIED MATERIALS & INTERFACES

www.acsami.org

Research Article

Role of the Interface between Ag and ZnO in the Electric Conductivity of Ag Nanoparticle-Embedded ZnO

Po-Shun Huang, Fen Qin, and Jung-Kun Lee*

Cite This: *ACS Appl. Mater. Interfaces* 2020, 12, 4715−4721

Read Online

ACCESS | Metrics & More | Article Recommendations | Supporting Information

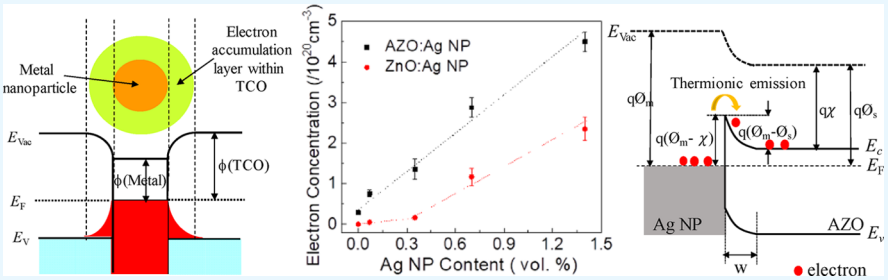

ABSTRACT: The addition of Ag nanoparticles (Ag NPs) with an average size of 30 nm into ZnO increases the electric conductivity up to 1000 times. While a similar increase in the conductivity is observed in a mixture of Ag nanoparticles and Al-doped ZnO (AZO) films, a physical mechanism underlying the change in electric conductivity is not the same for Ag NP-added ZnO and Ag NP-added AZO. In Ag NP-added ZnO, an ohmic junction is formed at the ZnO−Ag interface, and electrons are accumulated in ZnO near the ZnO−Ag interface until electron-rich islands are connected. However, in Ag NP-added AZO, electrons in Ag NPs move to the AZO matrix via thermionic emission and travel through the AZO matrix. This change in electron transport at ZnO−Ag and AZO−Ag interfaces is due to the fact that the work function of ZnO (4.62 eV) is larger than those of Ag (4.24 eV) and AZO (4.15 eV). An increase in Ag NP content in the ZnO matrix leads to the overlap of the electron accumulation regions and forms a percolation path for the electron transport without deteriorating the electron mobility. Hence, the electron concentration increases to $2.4 \times 10^{20}/\text{cm}^3$ in the 1.4 vol % Ag NP-added ZnO film. In addition, Ag NPs have a negligible effect on the transmittance, and the best Haacke figure of merit (Φ_H) values are 2.86 and 5.18 for ZnO:Ag NP and AZO:Ag NP, respectively.

KEYWORDS: *ZnO, Ag nanoparticles, metal−metal oxide interface, percolation, transparent conductor*

I. INTRODUCTION

Transparent conducting oxides (TCOs) are wide-band-gap (>3.0 eV) materials, which are doped with aliovalent elements. Therefore, TCOs are optically transparent for visible light and electrically conductive. Due to a unique combination of electric and optical properties, TCOs have been utilized as an electrode material of transparent thin-film transistors, photovoltaics, display panels, and touch screens.[1−10] Among a variety of TCO materials, indium tin oxide (ITO) films exhibit low sheet resistance and high transmittance. The sheet resistance values of ITO are 100 Ω/□ and 10 Ω/□ when the transmittance is 90 and 80%, respectively.[1−3,5−8] Despite ITO's excellent electric and optical properties, it has an inherent drawback resulting from scarcity of indium. An alternative is ZnO films doped with III-A metal group impurity (Al, Ga, and In). Zinc is more abundant than indium, and the electric conductivity of Al-doped ZnO is comparable to that of ITO.[1,4,9−15] One question about impurity-doped ZnO is whether the electron concentration can be increased without deteriorating the mobility. Since an electron concentration is proportional to the impurity-doping level in ZnO, a high concentration of donor impurities is necessary to increase the electron concentration of doped ZnO. However, the large amount of impurities in ZnO adversely affects the electron mobility. When donor impurities are activated in ZnO, they turn to positively charged defects and decrease the electron mobility by scattering free electrons. Electron mobility and concentration of impurity-doped ZnO in the literature are summarized in Figure 1.[11,12,16−23] It shows that the electron mobility becomes close to or smaller than 1 $\text{cm}^2/\text{V}\cdot\text{s}$ at the doping level of $10^{20}/\text{cm}^2$.

Several approaches have been proposed to circumvent an inherent conflict between carrier concentration and mobility in TCO. One of them is to insert nanostructured metals such as Au, Ag, or Cu into the TCO matrix.[16,21,24−31] A sandwich structure of composite films including the metal layer can be

Received: October 7, 2019
Accepted: December 30, 2019
Published: December 30, 2019

https://dx.doi.org/10.1021/acsami.9b17922
ACS Appl. Mater. Interfaces 2020, 12, 4715−4721

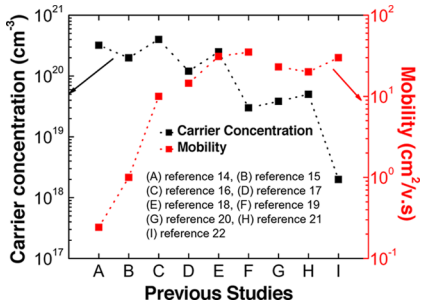

Figure 1. Carrier concentration and mobility of TCO films in the literature[14−22] showing that an increase in the carrier concentration generally decreases the carrier mobility.

electrically conductive and optically transparent. In this composite film, the continuous metal nanolayer is a major path for free electron transport. Recently, a different conduction mechanism in metal−TCO composite films has been reported. When a small amount of Au or Ag nanoparticles (NPs) was introduced into ZnO or the Al-doped ZnO matrix, an unconventional increment in the electron concentration (up to 10^{21} cm^{-3}) was observed.[28,29] This was explained by the thermionic emission of electrons at an interface between metal NPs and the ZnO matrix. Since the composite films do not need donor impurities for high electron concentration, the concentration of electrically charged scattering centers is low and the electron mobility is 10 $cm^2/V{\cdot}s$ or higher in a high electron concentration regime.

In this study, we examined the nature of the interface barrier between Ag NPs and the ZnO matrix in the electron transfer from Ag NPs to the ZnO matrix. Ag-doped ZnO and AZO films have been studied in the past. The focus of these previous studies was how Ag doping changes the electric and optical properties of ZnO and AZO films. Ag in the Zn site modifies the concentration and type of charge carriers and the optical band gap.[32,33] In contrast, in this study, Ag is not doped into ZnO or AZO. The film is a composite of Ag nanoparticles and ZnO (or AZO) films. From these composite films, it is found that the electron concentration is $2.4 \times 10^{20}/cm^3$ in the 1.4 vol % Ag NP-added ZnO film. To control the barrier type at the interface, the work function of the ZnO matrix was changed by doping 1.0 atom % Al into ZnO. The work function of silver ($Ø_{Ag}$) was found to be larger than that of ZnO ($Ø_{ZnO}$) but smaller than that of Al-doped ZnO ($Ø_{AZO}$).[31,34] Due to the work function difference, the energy barrier was different at the ZnO−Ag and AZO−Ag interfaces. This change in junction type, in return, changed the relation between electric conductivity and Ag NP content. In the case of the ohmic junction at the ZnO−Ag interface, an overlap of electron accumulation regions creates a percolation path where the electron concentration of the ZnO:Ag NP film is dramatically increased without a change in electron mobility. This leads to an increase in the electric conductivity of the ZnO:Ag NP film.

II. EXPERIMENTS

II.A. Preparation of ZnO and AZO Sol−Gel. The ZnO precursor was prepared by dissolving 0.75 M zinc acetate dehydrate in 40 mL of 2-methoxyethanol in a three-necked round flask. Monoethanolamine (MEA) was added to stabilize the precursor. For the AZO film, aluminum nitrate was added in the ZnO precursor as a source of donor impurity. The molar ratio of [Al] to [Zn] was 1:99. ZnO and AZO precursors were magnetically stirred at 80 °C for 1 h to obtain homogeneous and transparent sols. ZnO and AZO sols were both naturally cooled down to room temperature and aged for a day before Ag nanoparticles were added.

II.B. Synthesis of Ag Nanoparticles via a Polyol Method. Ag NPs were synthesized using a polyol method. Silver nitrate (20 mM; $AgNO_3$, 99.9999%) was dissolved in ethylene glycol (EG), which works not only as a solvent but also as a weak reducing agent. Polyvinylpyrrolidone (1 mM) was also added as a surfactant that controls the size and dispersion of Ag NPs. The solution was heated at 120 °C for 30 min under a constant N_2 flow to prevent the oxidation. The colorless Ag NP precursor immediately turned to a yellowish solution during the reaction. The color of the final Ag NP solution was light brown. The Ag NP solution was washed several times with acetone and centrifuged at 12,000 rpm for 30 min. Ag NPs collected from the centrifuge were redispersed in ethanol for further experiment. Transmission electron microscopy (TEM) images and UV−Vis absorption spectra of Ag NPs are shown in Figure S1. The average particle size of Ag NPs was 30.4 ± 8 nm, and the absorption peak of Ag NPs in ethanol was found at 395 nm.

II.C. Ag NP-Embedded ZnO and AZO Films. To prepare the coating solution, Ag NPs in ethanol were added to ZnO and AZO sols. A soda−lime glass was sonicated in acetone and ethanol for 10 min in sequence and then dried. The mixture solution was spin-coated multiple times at a rate of 3000 rpm on the soda−lime glass substrates until the film thickness reached ∼200 nm. AZO:Ag NP and ZnO:Ag NP films were annealed in nitrogen at 500 °C for 30 min to crystallize the oxide matrix. Then, films were treated in reducing ambience (95% N_2 mixed with 5% H_2) at 400 °C for 30 min to increase the electric conductivity. Scanning electron microscopy (SEM) images in Figure S2 show that the thickness of annealed films was 200 nm. Transmission electron microscopy (TEM) images of the 1.4 vol % Ag NP-embedded ZnO film are shown in Figure S3. This shows that Ag nanoparticles that are much smaller than 100 nm are uniformly distributed in the ZnO film.

II.D. Characterization of Crystal Structure and Electric Property. The crystal structures of mixture films were characterized by X-ray diffraction (XRD, X'Pert PANalytical) with Co Kα radiation of λ = 0.179 nm. The chemical state of embedded Ag NPs and the composition of AZO:Ag NP and ZnO:Ag NP films were analyzed using electron probe micro-analysis (EPMA). Table S1 shows the results of EPMA analysis. The Ag/Zn ratio was converted into volume ratio (vol %) since a minor phase content in composite materials is commonly expressed in volume percent. In Table S1, Ag NP contents in the ZnO matrix are rounded as 0.07, 0.35, 0.69, and 1.42 vol %. The oxidation status of Ag in ZnO and AZO matrices was characterized by X-ray photoelectron spectroscopy (XPS). Before XPS analysis was conducted, the surface of the films was sputtered for 10 s using 500 kV Ar ions to remove surface adsorbates. A peak position was calibrated using C 1s peak as an internal reference of 284.6 eV. Hall effect measurement (HMS-5000, Ecopia) and 4-probe resistivity measurement were performed to determine the carrier concentration and mobility of the films. The optical transmittance of the films was investigated by measuring the UV−Vis absorption spectra. The transmittance spectra of ZnO:Ag NP and AZO:Ag NP films are shown in Figure S4.

Basic materials properties of pure ZnO and AZO films such as resistivity, transmittance (at 550 nm), and mobility are summarized in Table S2. They are comparable to those of previous studies on sol−gel ZnO and AZO films.[18,35−38] To study the band structures at ZnO−Ag and AZO−Ag interfaces in AZO:Ag NP and ZnO:Ag NP films, the work functions of Ag, ZnO, and AZO films were probed using ultraviolet photoelectron spectroscopy (UPS) equipped with a UV source of He II ($h\nu$ = 40.6 eV). To accurately measure the work function of Ag, ZnO, and AZO near the metal/oxide interface, ZnO/Ag/ZnO and AZO/Ag/AZO multilayer films that mimicked ZnO:Ag NP and AZO:Ag NP films were prepared. Forty nanometer-thick semiconductor layers were spin-coated, and a 3 nm-thick Ag layer was deposited using electron beam evaporation. Before UPS analysis, the sandwich structure films were annealed at 500 °C in N_2, which was the annealing condition of ZnO:Ag NP and AZO:Ag NP films. During the measurement, the top semiconductor layer was sputtered

https://dx.doi.org/10.1021/acsami.9b17922
ACS Appl. Mater. Interfaces 2020, 12, 4715−4721

using 3 keV Ar^+ ions, and the gradual change in the photoemission peaks was monitored. To calibrate the UPS spectra, the Fermi level of a clean Au film was used as a reference.

III. RESULTS AND DISCUSSION

Figure S5 shows the XPS spectra of ZnO:Ag NP films with different Ag contents. The binding energy (BE) extracted from Ag $3d_{5/2}$ photoemission peaks is 368.04 eV in all films, which coincides with that of metallic Ag. In addition, an increase in Ag content does not change the BE of Zn−O bond. The BE of Ag and Zn peaks indicates that Ag is neither oxidized nor incorporated into ZnO during thermal treatment in N_2. The high stability of Ag NPs is attributed to the encapsulation effect of the ZnO matrix.

The crystal structure of ZnO:Ag NP films was investigated using XRD in a glancing angle geometry. XRD patterns are shown in Figure S6. Regardless of the Ag content, sol−gel-grown ZnO films have a hexagonal structure with a preferred orientation along the ⟨002⟩ direction. Ag NP addition does not shift ZnO (002) peak position, but the broadness of the (002) peak slightly increases in the 1.4 vol % ZnO:Ag NP film. This indicates that Ag is not incorporated into ZnO and the embedded Ag NPs produce a residual strain in the ZnO matrix. As Ag NP content becomes 0.7 vol % or higher, (111) and (200) peaks of cubic Ag are found at $2\theta = 44.6°$ and 52.5°, respectively. The appearance of metallic Ag in XRD patterns indicates that embedded Ag NPs are not oxidized during high-temperature thermal annealing in N_2, which is consistent with the result of XPS analysis.

The electron concentration of ZnO:Ag NP and AZO:Ag NP films was also investigated using Hall effect measurements and 4-probe resistivity measurement. Figure 2 shows a change in

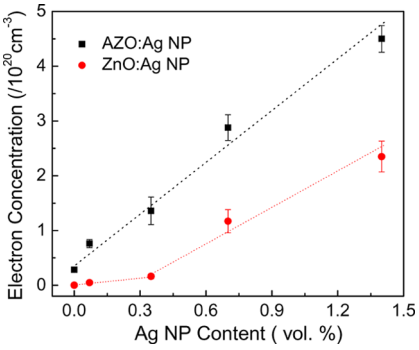

Figure 2. Electron concentration of AZO:Ag NP and ZnO:Ag NP films containing different volume percent values of Ag NPs.

the electron concentration of films as a function of Ag NP content. In ZnO:Ag NP films, as Ag NP content increases from 0 to 0.35 vol %, the carrier concentration increases marginally from $1.3 \times 10^{17}/cm^3$ to $1.6 \times 10^{19}/cm^3$. However, when Ag NP content is larger than 0.35 vol %, the electron concentration increases dramatically. The electron concentration of the ZnO:1.4 vol % Ag NP film is $2.4 \times 10^{20}/cm^3$, which is 1000 times larger than that of a pure ZnO film. In contrast, AZO:Ag NP films show a linear correlation between the Ag NP content and the electron concentration. The Ag NP increases the electron concentration of the AZO film by 15 times from $2.9 \times 10^{19}/cm^3$ (pure AZO film) to $4.5 \times 10^{20}/cm^3$ (1.4 vol % Ag NP-added AZO film). These different trends suggest that the effect of Ag NPs on the electron concentration depends on the composition of the oxide matrix.

To understand the different roles of ZnO and AZO matrices in the enhancement of the electron concentration, the Fermi energy level of Ag, ZnO, and AZO was examined by the UPS equipped with the excitation energies of He II ($h\nu$ = 40.6 eV). ZnO/Ag/ZnO and AZO/Ag/AZO multilayer films that mimicked ZnO:Ag NP and AZO:Ag NP films were chosen. Given that metal spheres and bulk have different work functions, the interface between Ag nanoparticles and ZnO needs to be examined to get the accurate work function.[39,40] The reason behind using the ZnO/Ag/ZnO multilayer to mimic the ZnO:Ag NP film is that the Ag nanolayer between sol−gel ZnO layers turns into a Ag nanoparticle film during the thermal annealing process. Because of high interface energy of the noble metal film−substrate, the metal thin film dewets during thermal annealing, and spherical nanoparticles are formed.[28,41,42] Therefore, the ZnO−Ag interface of the thermally annealed ZnO/Ag/ZnO multilayer is similar to that of ZnO:Ag NP films. During the measurement, the top oxide layer was sputtered until the Ag layer appeared. A change in the photoemission peak was monitored to determine the work functions of ZnO, AZO, and Ag at Ag/ZnO and Ag/AZO interfaces. To calibrate the UPS spectra, the Fermi level of a clean Au film was used as a reference. The work functions of ZnO, AZO, and Ag (ϕ_{ZnO}, ϕ_{AZO}, and ϕ_{Ag}) that were extracted from the secondary electron cut-off ($E_{S.O}$) (Figure S7) are 4.62, 4.15, and 4.24 eV, respectively. In addition, linear fitting toward the low binding energy edge shows that the highest valence band energy (E_v) values of ZnO and AZO are 7.45 and 7.37 eV below the vacuum energy level, respectively. In addition, from UV−Vis absorption measurement, the band gaps of pure ZnO and pure AZO turn out to be 3.3 and 3.4 eV at room temperature, respectively. A slightly larger band gap of AZO is due to the Moss−Burstein effect, which is often observed in degenerate semiconductors.[35] Based on these observations, the band structures of AZO−Ag and ZnO−Ag interfaces are plotted in Figure 3. Since the work function of Ag is larger than that of AZO, a Schottky barrier is formed at the AZO−Ag interface. In contrast, ZnO has larger work function than Ag, and there is no energetic barrier at the ZnO−Ag interface (i.e., ohmic junction).

The discrepancy in the interfacial junction can change the electron transport mechanism. Figure 4 schematically explains how free electrons inside Ag NPs move to ZnO and AZO matrices. In AZO:Ag NP films, the Schottky barrier regulates electron transfer at the interface. The thermionic emission allows electrons in Ag NPs to overcome the barrier and jump to the AZO matrix. Once free electrons jump to the AZO matrix, they move freely in the conduction band of AZO and increase the free electron concentration. In the ZnO−Ag NP interface, on the other hand, the ohmic junction is formed, and free electrons of Ag NPs are donated to the ZnO matrix at no energy cost. These surplus electrons in ZnO are accumulated near the ZnO−Ag interface due to bending of E_{Vac} of ZnO near the ZnO−Ag interface. The difference in the band structures of AZO:Ag and ZnO:Ag is schematically explained in Figure 7. The width of the electron accumulation region (W) of the ohmic junction at the oxide side is calculated using eq 1.[43,44]

$$W = \sqrt{\frac{2\varepsilon_0 \varepsilon_r k_B T}{q^2 n}} \quad (1)$$

https://dx.doi.org/10.1021/acsami.9b17922
ACS Appl. Mater. Interfaces 2020, 12, 4715−4721

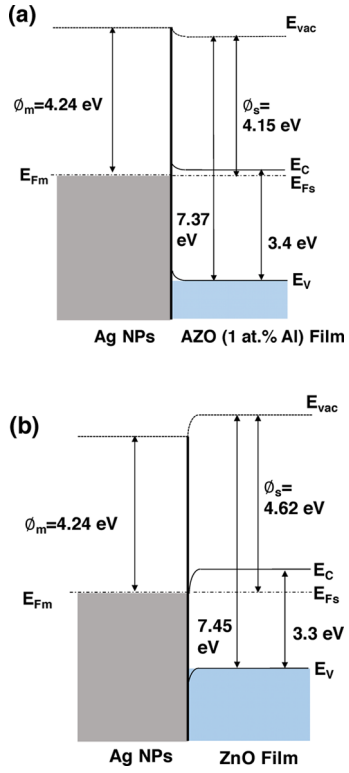

Figure 3. Equilibrium band diagrams of (a) AZO:Ag NP and (b) ZnO:Ag NP films.

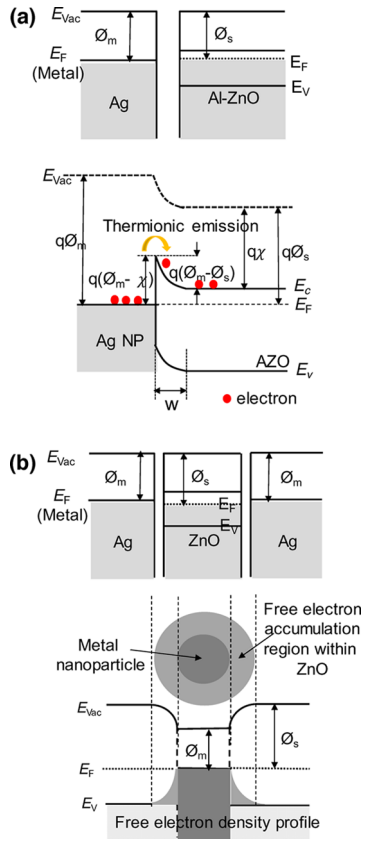

Figure 4. Schematics on the electron donation from metal nanoparticles to the oxide matrix at the interface of Ag NPs (a) with AZO and (b) with ZnO. (reproduced with permission from ref 29. Copyright 2017 American Chemical Society)

where ε_0 is the permittivity in free space, k_B is the Boltzmann constant, T is the temperature, q is the elemental electron charge, ε_r is the relative permittivity of undoped ZnO, and n is the charged impurity concentration.

According to eq 1, the electron accumulation width is estimated to be 25 nm from the ZnO−Ag interface toward the ZnO matrix. If Ag NPs are uniformly distributed in 0.1 vol % Ag NP-added ZnO, the center-to-center distance between Ag NPs and the volume ratio of the electron accumulation region are calculated as 242 nm and 1.8 vol %, respectively. This indicates that the electron accumulation regions surrounding Ag NPs are isolated from each other and surplus electrons of ZnO are confined near the ZnO−Ag NP interface. Therefore, when an amount of Ag NPs is less than 0.5 vol %, the free electron concentration of the ZnO:Ag NP film is much smaller than that of AZO:Ag NP film. In the 1.4 vol % Ag NP-added ZnO film, however, the center-to-center distance between Ag NPs is calculated as 100 nm, and the electron accumulation region occupies 25 vol % of the ZnO:Ag NP film that is close to a percolation threshold of spheres in three dimensions. This suggests that the electron accumulation regions can overlap to form a percolation path in the 1.4 vol % Ag NP-added ZnO film. The percolation path allows surplus electrons to flow under an electric field. This appearance of the channel of high electron density explains why the free electron concentration and electric conductivity of the ZnO:Ag NP film increase abruptly as the amount of Ag NPs increases from 0.4 to 1.4 vol %.

Figure 5 shows conductive atomic force microscopy (c-AFM) images of ZnO:Ag NP and AZO:Ag NP films. The measurement was performed in a contact mode, and +1.0 V DC bias was applied between the sample surface and a conducting AFM tip. In ZnO:Ag NP films, the electric current representing local electric conductivity varies significantly between measurement points. Localized conductive domains are observed, and the size of domains is smaller than 100 nm. In contrast, the c-AFM image of AZO:Ag NP films is very different from that of ZnO:Ag NP films. The variation of the electric current is much reduced, and the conductive domains are not localized. This different morphology of electrically conductive domains supports our hypothesis that the electron accumulation near the metal/oxide interface occurs only in ZnO:Ag NP films.

The effect of Ag NP content on the electron mobility of ZnO:Ag NP and AZO:Ag NP films also supports the idea on the formation of the percolation path. Figure 6 shows the mobility of ZnO:Ag NP films. The electron mobility of 1.4 vol % Ag NP-added ZnO is 32 $cm^2/V{\cdot}s$, which is almost the same as that of pure ZnO (34 $cm^2/V{\cdot}s$). Given that the electron concentration increases 3 orders of magnitude by adding 1.4 vol % of Ag NPs, a negligible difference in the mobility between pure ZnO and ZnO:Ag NP films was not expected. For instance, in n-type Si, an increase in the electron concentration from $10^{17}/cm^3$ to $10^{20}/cm^3$ accompanies a decrease in the mobility by 10 times, which is due to the donor impurity scattering. However, additional impurities are not added to the ZnO matrix of the ZnO:Ag NP film. Instead of the impurity doping, the percolation path of the electron accumulation region in the ZnO matrix allows the transport and free electrons through the ZnO matrix of ZnO:Ag NP films. Therefore, pure ZnO and ZnO:Ag films have a similar collision length of free electrons, and their electron mobility is almost same. The mobility of AZO:Ag NP films is lower than

https://dx.doi.org/10.1021/acsami.9b17922
ACS Appl. Mater. Interfaces 2020, 12, 4715−4721

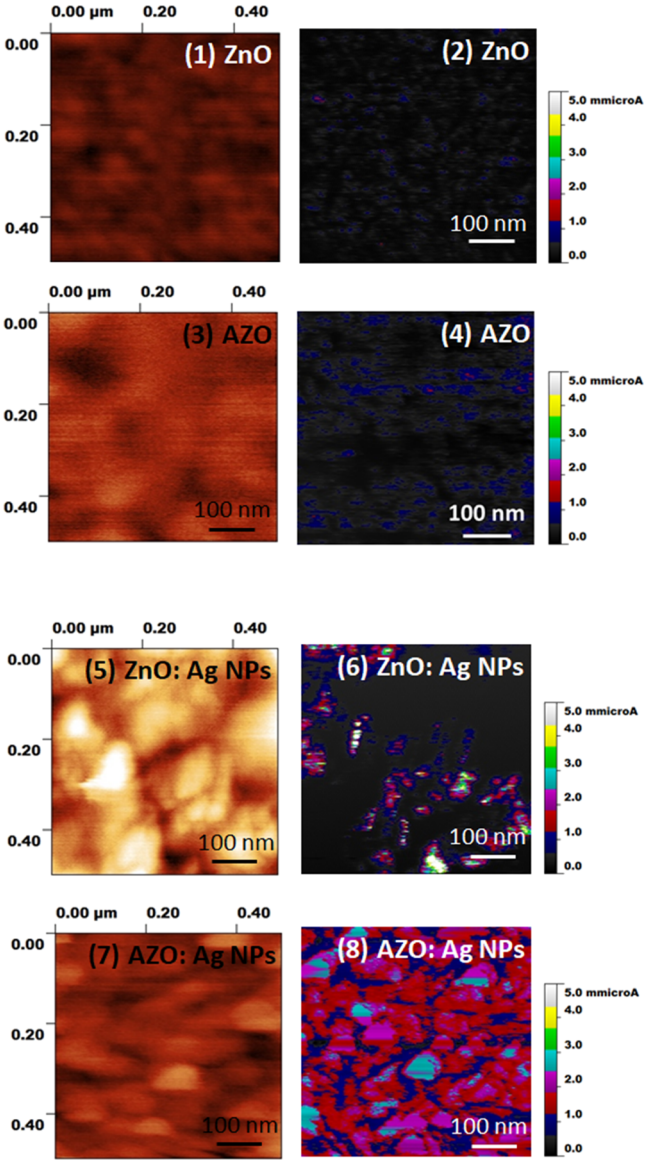

Figure 5. AFM images of (1) ZnO, (3) AZO, (5) ZnO:Ag NPs, and (7) AZO:Ag NPs and c-AFM images of (2) ZnO, (4) AZO, (6) ZnO:Ag NPs, and (8) AZO:Ag NPs.

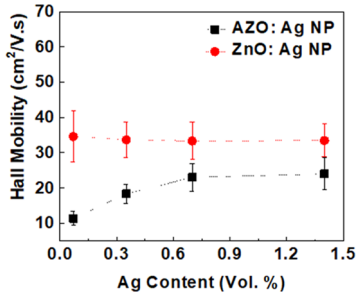

Figure 6. Hall mobility of ZnO:Ag NP and AZO:Ag NP films as a function of Ag NP content.

that of ZnO:Ag NP films due to the ionized Al impurities in AZO, although an increase in Ag content does not decrease the mobility of AZO:Ag NP films. The effect of Ag NP content on the mobility of AZO:Ag NP films can be explained by a change in the Fermi energy level. An increase in Ag NP content increases the Fermi energy level and neutralizes donor impurities, which would have been activated in a pure AZO film. In comparison to activated impurities, the neutral impurities have a much smaller electron scattering cross section, and the effect of Al impurities on the mobility of the AZO matrix is reduced.[29,45,46]

Figure 7 shows optical transmittances (λ = 550 nm) versus sheet resistance of ZnO:Ag NP and AZO:Ag NP films.

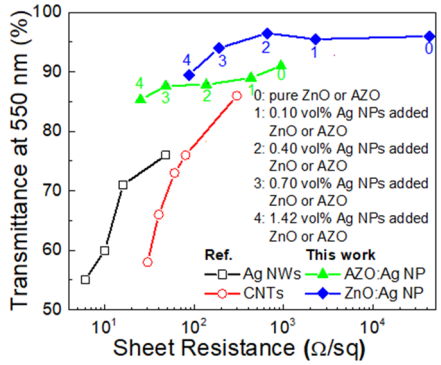

Figure 7. Transmittance versus sheet resistance of ZnO:Ag NP and AZO:Ag NP films (properties of Ag NW and CNT films in references are also plotted).

Previous results on transparent conductors are also included as a reference.[47] The optical transmittance is above 90% for ZnO:Ag NP films. An increase in Ag NP content slightly decreases the optical transmittance, which is attributed to light scattering by Ag NPs. The transmittance of AZO:Ag NP films is in the range of 86−90%. A few percent decrease in the transmittance of AZO:Ag NP films is due to the fact that the addition of Al into ZnO forms a defect center such as oxygen vacancies. The figure of merits (FOM) of the films was calculated using Haacke's method.[48] The best FOM values of ZnO:Ag NP and AZO:Ag NP films are 2.86 × $10^{-2}/\Omega$ and 5.18 × $10^{-2}/\Omega$, respectively. These values are larger than the FOM of Ag NW-based transparent electrode (FOM = 1.34 × $10^{-2}/\Omega$) and that of CNT-based transparent electrodes (FOM = 0.74 × $10^{-2}/\Omega$).[47]

IV. CONCLUSIONS

The addition of Ag NPs into ZnO and AZO films increases the electric conductivity of films via different mechanisms due to different work functions of ZnO and AZO. While ohmic contact is formed for the ZnO−Ag interface, a Schottky barrier is found at the AZO−Ag interface. This leads to different roles of Ag NPs in the electric conductivity of ZnO:Ag NP and AZO:Ag NP films. In the ZnO:Ag NP film, excess electrons are accumulated in the ZnO matrix near Ag NPs, and an increase in Ag NP content causes the appearance of the percolation path consisting of the electron accumulation region. The high electric conductivity of the ZnO:Ag NP film is attributed to this percolation path. In contrast, electrons in Ag NPs that overcome the Schottky barrier at the interface through thermionic emission can travel freely in the AZO matrix and contribute to electric conductivity. Transmittance of ZnO and AZO films embedded with 0.7 vol % Ag NPs is 85% or higher for visible light at the 550 nm wavelength. The best Haacke FOM values of ZnO:Ag NP and AZO:Ag NP films are 2.85 and 5.18, which show their promising potential as new transparent conductors.

https://dx.doi.org/10.1021/acsami.9b17922
ACS Appl. Mater. Interfaces 2020, 12, 4715−4721

■ ASSOCIATED CONTENT

Supporting Information

The Supporting Information is available free of charge at https://pubs.acs.org/doi/10.1021/acsami.9b17922.

EPMA analysis results, TEM image, Ag nanoparticle size distribution, UV−Vis absorption spectra, and SEM images (PDF)

■ AUTHOR INFORMATION

Corresponding Author

Jung-Kun Lee − *University of Pittsburgh, Pittsburgh, Pennsylvania;* orcid.org/0000-0002-7778-7679; Email: jul37@pitt.edu

Other Authors

Po-Shun Huang − *University of Pittsburgh, Pittsburgh, Pennsylvania*

Fen Qin − *University of Pittsburgh, Pittsburgh, Pennsylvania*

Complete contact information is available at: https://pubs.acs.org/10.1021/acsami.9b17922

Notes

The authors declare no competing financial interest.

■ ACKNOWLEDGMENTS

This work was supported by the National Science Foundation (NSF 1709307), National Research Foundation of Korea (NRF) grant funded by the Korea goverment (MSIP) (NRF-2016M1A2A2940138) and Global Frontier R&D Program on Center for Multiscale Energy System, Korea (2012M3A6A7054855).

■ REFERENCES

(1) Afre, R. A.; Sharma, N.; Sharon, M.; Sharon, M. Transparent Conducting Oxide Films for Various Applications: A review. *Rev. Adv. Mater. Sci.* **2018**, *53*, 79−89.

(2) Exarhos, G. J.; Zhou, X.-D. Discovery-based Design of Transparent Conducting Oxide Films. *Thin Solid Films* **2007**, *515*, 7025−7052.

(3) Fortunato, E.; Ginley, D.; Hosono, H.; Paine, D. C. Transparent Conducting Oxides for Photovoltaics. *MRS Bull.* **2007**, *32*, 242−247.

(4) Giang Nguyen, N.; Thanh Ho, V. T.; Hong, L.-S. Low-resistivity, High-transmittance Ga: ZnO Films Prepared Through Metalorganic Chemical Vapor Deposition Using an Inexpensive Solution of Diethylzinc in N-hexane as the Zn Precursor. *Appl. Phys. Lett.* **2013**, *102*, 181912.

(5) Gordon, R. G. Criteria for Choosing Transparent Conductors. *MRS Bull.* **2000**, *25*, 52−57.

(6) Granqvist, C. G.; Hultåker, A. Transparent and Conducting ITO Films: New Developments and Applications. *Thin Solid Films* **2002**, *411*, 1−5.

(7) Liu, H.; Avrutin, V.; Izyumskaya, N.; Özgür, Ü.; Morkoç, H. Transparent Conducting Oxides for Electrode Applications in Light Dmitting and Absorbing Devices. *Superlattices Microstruct.* **2010**, *48*, 458−484.

(8) Minami, T. Present Status of Transparent Conducting Oxide Thin-film Development for Indium-Tin-Oxide (ITO) Substitutes. *Thin Solid Films* **2008**, *516*, 5822−5828.

(9) Shirakata, S.; Sakemi, T.; Awai, K.; Yamamoto, T. Electrical and Optical Properties of Large Area Ga-doped ZnO Thin Films Prepared by Reactive Plasma Deposition. *Superlattices Microstruct.* **2006**, *39*, 218−228.

(10) Tsang, W. M.; Wong, F. L.; Fung, M. K.; Chang, J. C.; Lee, C. S.; Lee, S. T. Transparent Conducting Aluminum-doped Zinc Oxide Thin Film Prepared by Sol−gel Process Followed by Laser Irradiation Treatment. *Thin Solid Films* **2008**, *517*, 891−895.

(11) Chen, K. J.; Hung, F. Y.; Chang, S. J.; Hu, Z. S. Microstructures, Optical and Electrical Properties of In-doped ZnO Thin Films Prepared by Sol−gel Method. *Appl. Surf. Sci.* **2009**, *255*, 6308−6312.

(12) Gómez, H.; Olvera, M. D. L. L. Ga-doped ZnO Thin Films: Effect of Deposition Temperature, Dopant Concentration, and Vacuum-thermal Treatment on the Electrical, Optical, Structural and Morphological Properties. *Mater. Sci. Eng., B* **2006**, *134*, 20−26.

(13) Gonçalves, G.; Elangovan, E.; Barquinha, P.; Pereira, L.; Martins, R.; Fortunato, E. Influence of Post-annealing Temperature on the Properties Exhibited by ITO, IZO and GZO Thin Films. *Thin Solid Films* **2007**, *515*, 8562−8566.

(14) Janotti, A.; Van de Walle, C. G. Fundamentals of Zinc Oxide as a Semiconductor. *Rep. Prog. Phys.* **2009**, *72*, 126501.

(15) Wu, Y.; Hermkens, P. M.; Van De Loo, B. W. H.; Knoops, H. C. M.; Potts, S. E.; Verheijen, M. A.; Roozeboom, F.; Kessels, W. M. M. Electrical Transport and Al Doping Efficiency in Nanoscale ZnO Films Prepared by Atomic Layer Deposition. *J. Appl. Phys.* **2013**, *114*, No. 024308.

(16) Lee, S.; Bang, S.; Park, J.; Park, S.; Ko, Y.; Jeon, H. AZO/Au/AZO Multilayer as a Transparent Conductive Electrode. *Phys. Status Solidi A* **2012**, *209*, 698−701.

(17) Lee, S.-Y.; Park, B.-O. Electrical and Optical Properties of In_2O_3−ZnO Thin Films Prepared by Sol−gel Method. *Thin Solid Films* **2005**, *484*, 184−187.

(18) Lin, J.-P.; Wu, J.-M. The Effect of Annealing Processes on Electronic Properties of Sol-gel Derived Al-doped ZnO films. *Appl. Phys. Lett.* **2008**, *92*, 134103.

(19) Lin, K.-m.; Chen, H.-C.; Chen, Y.-Y.; Chou, K.-y. Influences of Preferred Orientation Growth on Electrical Properties of ZnO: Al films by Sol−gel Method. *J. Sol-Gel Sci. Technol.* **2010**, *55*, 369−376.

(20) Lin, K.-m.; Chen, Y.-Y.; Chou, K.-Y. Solution Derived Al-doped Zinc Oxide Films: Doping Effect, Microstructure and Electrical Property. *J. Sol-Gel Sci. Technol.* **2009**, *49*, 238−242.

(21) Sivaramakrishnan, K.; Alford, T. L. Conduction and Transmission Analysis in Gold Nanolayers Embedded in Zinc Oxide for Flexible Electronics. *Appl. Phys. Lett.* **2010**, *96*, 201109.

(22) Wang, H.; Xu, M.-h.; Xu, J.-w.; Ren, M.-f.; Yang, L. Low Temperature Synthesis of Sol−gel Derived Al-doped ZnO Thin Films with Rapid Thermal Annealing Process. *J. Mater. Sci.: Mater. Electron.* **2010**, *21*, 589−594.

(23) Yu, Q.; Fu, W.; Yu, C.; Yang, H.; Wei, R.; Sui, Y.; Liu, S.; Liu, Z.; Li, M.; Wang, G.; Shao, C.; Liu, Y.; Zou, G. Structural, Electrical and Optical Properties of Yttrium-doped ZnO Thin Films Prepared by Sol−gel method. *J. Phys. D: Appl. Phys.* **2007**, *40*, 5592.

(24) Gao, T.; Huang, P.-S.; Lee, J.-K.; Leu, P. W. Hierarchical Metal Nanomesh/microgrid Structures for High Performance Transparent Electrodes. *RSC Adv.* **2015**, *5*, 70713−70717.

(25) Han, H.; Theodore, N. D.; Alford, T. L. Improved Conductivity and Mechanism of Carrier Transport in Zinc Oxide with Embedded Silver Layer. *J. Appl. Phys.* **2008**, *103*, No. 013708.

(26) Houng, B. Tin Doped Indium Oxide Transparent Conducting Thin Films Containing Silver Nanoparticles by Sol-gel Technique. *Appl. Phys. Lett.* **2005**, *87*, 251922.

(27) Huang, P.-S.; Gao, T. Current Development of 1D and 2D Metallic Nanomaterials for the Application of Transparent Conductors in Solar Cells: Fabrication and Modeling. *Nano-Struct. Nano-Objects* **2018**, *15*, 119−139.

(28) Huang, P.-S.; Hoe Kim, D.; Lee, J.-K. Electron Emission of Au Nanoparticles Embedded in ZnO for Highly Conductive Oxide. *Appl. Phys. Lett.* **2014**, *104*, 142102.

(29) Huang, P.-S.; Qin, F.; Xiong, Z.; Shim, H.-W.; Gao, T.; Leu, P.; Lee, J.-K. Novel Carrier Doping Mechanism for Transparent Conductor: Electron Donation from Embedded Ag Nanoparticles

to the Oxide Matrix. *ACS Appl. Mater. Interfaces* **2017**, *9*, 19973−19979.
(30) Kim, A.; Won, Y.; Woo, K.; Kim, C.-H.; Moon, J. Highly Transparent Low Resistance ZnO/Ag Nanowire/ZnO Composite Electrode for Thin Film Solar Cells. *ACS Nano* **2013**, *7*, 1081−1091.
(31) Uda, M.; Nakamura, A.; Yamamoto, T.; Fujimoto, Y. Work Function of Polycrystalline Ag, Au and Al. *J. Electron Spectrosc. Relat. Phenom.* **1998**, *88-91*, 643−648.
(32) Li, W. J.; Kong, C. Y.; Ruan, H. B.; Qin, G. P.; Huang, G. J.; Yang, T. Y.; Liang, W. W.; Zhao, Y. H.; Meng, X. D.; Yu, P.; Cui, Y. T.; Fang, L. Electrical Properties and Raman Scattering Investigation of Ag Doped ZnO Thin Films. *Solid State Commun.* **2012**, *152*, 147−150.
(33) Acharya, A. D.; Sarwan, B.; Panda, R.; Shrivastava, S. B.; Ganesan, V. Tuning of TCO Properties of ZnO by Silver Addition. *Superlattices Microstruct.* **2014**, *67*, 97−109.
(34) Schnippering, M.; Carrara, M.; Foelske, A.; Kötz, R.; Fermín, D. J. Electronic Properties of Ag Nanoparticle Arrays. A Kelvin Probe and High Resolution XPS Study. *Phys. Chem. Chem. Phys.* **2007**, *9*, 725−730.
(35) Caglar, M.; Ruzgar, S. Influence of the Deposition Temperature on the Physical Properties of High Electron Mobility ZnO films by Sol−gel Process. *J. Alloys Compd.* **2015**, *644*, 101−105.
(36) Paul, G. K.; Bandyopadhyay, S.; Sen, S. K.; Sen, S. Structural, Optical and Electrical Studies on Sol−gel Deposited Zr Doped ZnO Films. *Mater. Chem. Phys.* **2003**, *79*, 71−75.
(37) Schuler, T.; Aegerter, M. A. Optical, Electrical and Structural Properties of Sol Gel ZnO: Al Coatings. *Thin Solid Films* **1999**, *351*, 125−131.
(38) Bong, H.; Lee, W. H.; Lee, D. Y.; Kim, B. J.; Cho, J. H.; Cho, K. High-mobility Low-Temperature ZnO Transistors with Low-voltage Operation. *Appl. Phys. Lett.* **2010**, *96*, 192115.
(39) Zhou, L.; Zachariah, M. R. Size Resolved Particle Work Function Measurement of Free Nanoparticles: Aggregates vs. Spheres. *Chem. Phys. Lett.* **2012**, *525-526*, 77−81.
(40) Wood, D. M. Classical Size Dependence of the Work Function of Small Metallic Spheres. *Phys. Rev. Lett.* **1981**, *46*, 749.
(41) Thompson, C. V. Solid-state Dewetting of Thin Films. *Annu. Rev. Mater. Res.* **2012**, *42*, 399−434.
(42) Niekiel, F.; Schweizer, P.; Kraschewski, S. M.; Butz, B.; Spiecker, E. The Process of Solid-State Dewetting of Au Thin Films Studied by *In Situ* Scanning Transmission Electron Microscopy. *Acta Mater.* **2015**, *90*, 118−132.
(43) Hong Noh, J.; Ding, B.; Soo Han, H.; Seong Kim, J.; Hoon Park, J.; Baek Park, S.; Suk Jung, H.; Lee, J.-K.; Sun Hong, K. Tin Doped Indium Oxide Core—TiO_2 Shell Nanowires on Stainless Steel Mesh for Flexible Photoelectrochemical Cells. *Appl. Phys. Lett.* **2012**, *100*, No. 084104.
(44) Kumar, C.; Kim, D. M. *Introductory Quantum Mechanics for Semiconductor Nanotechnology*; John Wiley & Sons, 2015.
(45) Agashe, C.; Kluth, O.; Hüpkes, J.; Zastrow, U.; Rech, B.; Wuttig, M. Efforts to Improve Carrier Mobility in Radio Frequency Sputtered Aluminum Doped Zinc Oxide Films. *J. Appl. Phys.* **2004**, *95*, 1911−1917.
(46) Pei, Z. L.; Sun, C.; Tan, M. H.; Xiao, J. Q.; Guan, D. H.; Huang, R. F.; Wen, L. S. Optical and Electrical Properties of Direct-current Magnetron Sputtered ZnO: Al films. *J. Appl. Phys.* **2001**, *90*, 3432−3436.
(47) Barnes, T. M.; Reese, M. O.; Bergeson, J. D.; Larsen, B. A.; Blackburn, J. L.; Beard, M. C.; Bult, J.; Van de Lagemaat, J. Comparing the Fundamental Physics and Device Performance of Transparent, Conductive Nanostructured Networks with Conventional Transparent Conducting Oxides. *Adv. Energy Mater.* **2012**, *2*, 353−360.
(48) Haacke, G. New Figure of Merit for Transparent Conductors. *J. Appl. Phys.* **1976**, *47*, 4086−4089.

https://dx.doi.org/10.1021/acsami.9b17922
ACS Appl. Mater. Interfaces 2020, 12, 4715−4721